Built-in field control in alloyed c-plane III-N quantum dots and wells

M. A. Caro' , S. Schulz, S. B. Healy, and E. P. O'Reilly

Citation: Journal of Applied Physics **109**, 084110 (2011); doi: 10.1063/1.3563568
View online: http://dx.doi.org/10.1063/1.3563568
View Table of Contents: http://aip.scitation.org/toc/jap/109/8
Published by the American Institute of Physics

Built-in field control in alloyed *c*-plane III-N quantum dots and wells

M. A. Caro,[1,2,a)] S. Schulz,[1] S. B. Healy,[1] and E. P. O'Reilly[1,2]
[1]*Tyndall National Institute, Lee Maltings, Cork, Ireland*
[2]*Department of Physics, University College Cork, Cork, Ireland*

(Received 23 September 2010; accepted 1 February 2011; published online 22 April 2011)

We investigate the degree to which the built-in electric field can be suppressed by employing polarization-matched barriers in III-N quantum well and dot structures grown along the *c* axis. Our results show that it is possible to take advantage of the opposite contributions to the built-in potential arising from the different possible combinations of wurtzite GaN, InN, and AlN when alloying the materials. We show that, for a fixed bandgap of the dot/well, optimal alloy compositions can be found that minimize the built-in field across the structure. We discuss and study the impact of different material parameters on the results, including the influence of nonlinear effects in the piezoelectric polarization. Structures grown with unstrained barriers and on GaN epilayers are considered, including discussion of the effects of constraints such as strain limits and alloy miscibility. © *2011 American Institute of Physics*. [doi:10.1063/1.3563568]

I. INTRODUCTION

Group III nitrides have attracted great attention over the last few years due to their potential for optoelectronic applications given the wide energy range over which their bandgap E_g spans.[1] Alloying InN, GaN, and AlN can allow access to the whole optical spectrum, from near infrared (IR) to the ultraviolet (UV). InGaN-based devices have been demonstrated and proven to be a reliable solution for lighting applications in the blue part of the spectrum ($E_g \sim 2.7$ eV).[2,3] However, technical challenges still remain present, including for example the growth of high-quality In-rich InGaN systems, which would allow the implementation of efficient solutions for green, yellow and amber light emitting diodes (LED) and lasers ($E_g \sim 2.0$–2.5 eV).[3–5] UV radiation sources ($E_g > 3.4$ eV)[1] are of interest for various applications such as optical storage, medical diagnostics and treatment, and sterilization processes.[6,7] In this spectral range, nitride-based structures might be either a good candidate for the replacement of traditional low-efficiency devices, or the only available solution in environments where it is not possible to implement any alternative approach.[6–8] Although there have been great improvements in the quality of nitride-based materials and structures during the past two decades, there is still need for further improvement toward the goal of high efficiency devices.[3,9]

Even though it is possible under certain conditions to grow III-N materials in the zinc-blende phase,[10,11] they usually crystallize in the wurtzite structure. One of the particularities of this structure for group-III nitrides is the existence of spontaneous electric dipoles along the [0001] direction (*c*-axis) of the lattice, due to the highly ionic character of the bonds and the lack of an inversion plane perpendicular to the *c*-axis.[12] Along with this *spontaneous polarization*, additional dipoles are created when the material undergoes strain, generating the so-called *piezoelectric polarization*.[13] The total polarization differs for different nitrides, thus giving rise to the accumulation of interfacial electric charges in nitride-based heterostructures. This accumulation is particularly important in the cases where the crystal growth axis coincides with the *c*-axis. Because it is more difficult to achieve crystals of high quality for nitride systems grown on nonpolar substrates,[14] *c*-plane nitrides remain the usual choice when trying to construct semiconductor nanostructures such as quantum wells (QWs) and quantum dots (QDs). Therefore, the charge accumulation remains a problem.

The main consequence of this interfacial charge accumulation is the large built-in electric field present in heterostructures where wurtzite nitrides are employed. Among other explanations, including Auger recombination[15] and defect-related delocalization of carriers,[16] it has been suggested that these built-in fields are the origin of the dramatic *efficiency droop* observed as the drive current is increased in GaN-based multiple quantum well LEDs.[17,18] The built-in field leads to spatial separation of the electrons and holes in heterostructures, and to a dramatic reduction in the optical recombination rate.[19,20] In order to overcome this charge carrier separation, Kim *et al.*[17] proposed the use of polarization-matched barriers and InGaN QWs. Later on, the same group of researchers reported an enhanced performance of those structures by using partially polarization-matched barriers.[21–23] We present here a generalization of that concept and investigate the potential for polarization-matching and minimization of built-in fields in III-N QW and QD structures.

We start in Sec. II A with a brief introduction to the methods we use to calculate the built-in fields in QW and QD structures. A discussion of different interpolation methods for the relevant material parameters in nitride alloys (including the elastic and piezoelectric properties) is presented in Sec. II B. Section III overviews the principles behind the concept of *built-in field control* and then presents the field suppression results for nitride systems grown both with unstrained barriers and also with barriers strained to the in-plane lattice constant of an underlying GaN substrate. This analysis is extended in Sec. III D to consider experimentally observed constraints, including strain relaxation and alloy miscibility issues. Finally we summarize and present our conclusions in Sec. IV.

[a)]Electronic mail: mcaroba@gmail.com.

II. CALCULATION OF THE BUILT-IN FIELD

A. Built-in potential in quantum dots and wells

In the case of a QW, simple arguments can be employed to obtain the polarization potential $\varphi^{\mathrm{QW}}(z)$ along the growth direction ([0001] direction or c-axis) as a function of both spontaneous and strain-related piezoelectric polarization vectors. Assuming that stress is applied in the basal plane only, both the spontaneous $\mathbf{P}_{\mathrm{sp}} = P_{\mathrm{sp}}\hat{\mathbf{z}}$ and piezoelectric polarizations $\mathbf{P}_{\mathrm{pz}} = P_{\mathrm{pz}}\hat{\mathbf{z}}$ are constant vectors along the [0001] direction within the QW and within the barrier.[13] In the following, the z axis will be always considered to be parallel to the [0001] direction. The total built-in potential $\varphi^{\mathrm{QW}}(z)$ within the QW is given by:

$$\varphi^{\mathrm{QW}}(z) = \varphi_{\mathrm{sp}}^{\mathrm{QW}}(z) + \varphi_{\mathrm{pz}}^{\mathrm{QW}}(z) = \left\{\frac{(P_{\mathrm{sp}}^{\mathrm{W}} - P_{\mathrm{sp}}^{\mathrm{B}}) + P_{\mathrm{pz}}^{\mathrm{W}}}{2\epsilon_0\epsilon_r^{\mathrm{W}}}\right\}(|z| - |z-h|), \quad (1)$$

where the QW is of height h, with interfaces at $z = 0$ and $z = h$, ϵ_r^{W} is the QW dielectric constant, and the piezoelectric polarization vector $P_{\mathrm{pz}}^{\mathrm{W}}$ in the QW is given by[13]

$$P_{\mathrm{pz}}^{\mathrm{W}} = 2\varepsilon_{11}e_{31}^{\mathrm{W}} + \varepsilon_{33}e_{33}^{\mathrm{W}} \quad (2)$$

with

$$\varepsilon_{33} = -2\frac{C_{13}^{\mathrm{W}}}{C_{33}^{\mathrm{W}}}\varepsilon_{11}. \quad (3)$$

The well and the barrier are denoted with the indices W and B, respectively, $\varepsilon_{11} = (a_{\mathrm{B}} - a_{\mathrm{W}})/a_{\mathrm{W}}$ is the basal strain, ε_{33} the strain along the c-axis, e_{ij} are the piezoelectric coefficients and C_{ij} are the elastic constants.

The calculation of the total built-in potential φ in a QD is more complicated because the piezoelectric polarization vector is no longer a constant vector along the [0001] direction within the QD and within the barrier. To calculate the polarization potential in nitride-based QDs we apply a real-space surface integral approach developed by Williams *et al.*[24] This method admits analytical solutions in certain cases and provides an extremely useful insight into the parameters that influence the magnitude and the shape of the polarization potential. In this work, we use the solutions obtained in Ref. 24 for a line-scan of the potential $\varphi^{\mathrm{QD}}(z)$ along the z-direction through the center of a truncated-cone shaped QD. Using the notation of Ref. 24, $\varphi^{\mathrm{QD}}(z)$ can be found along the central axis ($x = y = 0$) by evaluating the following surface integrals:

$$\varphi^{\mathrm{QD}}(z) = JI_1 + \left[\frac{P_{\mathrm{sp}}^{\mathrm{D}} - P_{\mathrm{sp}}^{\mathrm{B}}}{4\pi\epsilon_0\epsilon_r} + K\right]I_2, \quad (4)$$

where

$$I_1 = \int_{\mathrm{QD}} \frac{(z-z')^2}{\left[x'^2 + y'^2 + (z-z')^2\right]^{\frac{3}{2}}}\hat{\mathbf{z}}\cdot d\mathbf{s}'$$
$$I_2 = \int_{\mathrm{QD}} \frac{1}{\left[x'^2 + y'^2 + (z-z')^2\right]^{\frac{1}{2}}}\hat{\mathbf{z}}\cdot d\mathbf{s}', \quad (5)$$

and where D refers to the dot and B to the barrier. The analytical solution for these integrals, as well as an expression for the material- and strain-dependent coefficients J and K, is given in Ref. 24.

Finally, the built-in field $E(z)$ corresponding to the potentials given in Eqs. (1) and (4) is calculated as the derivative of φ with respect to the variable z:

$$E(z) = -\frac{d\varphi(z)}{dz}. \quad (6)$$

Because the piezoelectric potential arises from the strain-induced polarization, it is crucial to correctly identify which are the straining and strained layers. In Secs. III A and III B we consider the ideal case in which only a well (or dot) and barrier are present in the structure. Since the dot is completely embedded in the barrier, the relaxation mechanisms in QDs and their consequences for the piezoelectric potential are complex and have to be modeled using Eq. (4). In contrast, the description of strain relaxation and its consequences is much simpler for a QW, with the well relaxing along the c-axis as in Eq. (3) and with the barrier remaining strain-free. In Sec. III C we extend the analysis to consider the case where the structures are grown on a GaN buffer layer and, therefore, both barrier and well (or dot) experience a modified strain to account for the lattice mismatch with respect to the substrate.

B. Nitride alloy material parameters

Although the calculation of the potentials in Eqs. (1) and (4) is straight-forward, the value of the material-dependent constants involved in those equations is not so well established. In their review paper from 2003, Vurgaftman and Meyer[25] give a range of parameter values found in the literature for the nitride binaries and propose a best choice. Even though their compilation has probably been the set of parameters most widely used by the community over the last few years, the progress in the knowledge of the properties of nitride materials make some of these values inevitably obsolete and a certain degree of revision is desirable.

Some controversy surrounds the sign of the piezoelectric coefficient e_{15}, which is of relative importance in the calculation of the piezoelectric potential in QDs. Further discussion on this issue as well as experimental evidence that supports the use of a negative value for e_{15} can be found in Refs. 30 and 31. Here, we apply the piezoelectric coefficients of Shimada,[26] who derives a negative sign for e_{15} and obtains values of e_{31} and e_{33} in line with those reported by Vurgaftman and Meyer.[25] The spontaneous polarization values are also taken from Ref. 25. The dielectric constants are taken from Wagner *et al.*[27] for GaN and AlN, and Furthmüller *et al.*[28] for InN. The parameter values which we use for nitride binaries are listed in Table I.

The parameters for ternary and quaternary alloys are in general less well known. In the absence of knowledge on the dependence with composition of a particular parameter, it is usual to take a linear interpolation of the binary values:

$$\xi(\mathrm{Al}_x\mathrm{In}_y\mathrm{Ga}_{1-x-y}\mathrm{N}) = x\xi(\mathrm{AlN}) + y\xi(\mathrm{InN}) + (1-x-y)\xi(\mathrm{GaN}). \quad (7)$$

TABLE I. If not indicated otherwise, all material parameters for the wurtzite nitride binaries are taken from Ref. 25. The energy gap of GaN and AlN at $T = 300$ K is estimated by using the Varshni formula and the parameters reported in Ref. 25.

	GaN	AlN	InN
E_g (eV) at $T = 300$ K	3.44	6.16	0.64[d]
a (Å) at $T = 300$ K	3.189	3.112	3.545
c (Å) at $T = 300$ K	5.185	4.982	5.703
P_{sp} (C/m^2)	− 0.034	− 0.090	− 0.042
e_{15} (C/m^2)	− 0.38[a]	− 0.41[a]	− 0.44[a]
e_{31} (C/m^2)	− 0.45[a]	− 0.45[a]	− 0.52[a]
e_{33} (C/m^2)	0.83[a]	1.54[a]	0.95[a]
C_{12} (GPa)	145	137	115
C_{13} (GPa)	106	108	92
C_{33} (GPa)	398	373	224
C_{44} (GPa)	105	116	48
ϵ_r (F/m)	9.6[b]	8.5[b]	7.2[c]

[a]Reference 26.
[b]Reference 27.
[c]Reference 28.
[d]Reference 29.

Equation (7) is known as Végard's law. It is widely used for the calculation of general nitride parameters, such as the lattice constants,[25,32] and has also been used to estimate built-in fields in $A_xB_{1-x}N$ QDs.[24,33] Where more detailed information is known, it can be useful for some $A_xB_{1-x}N$ parameters to use a quadratic interpolation between the values of the binaries AN and BN via the introduction of the so called bowing parameter b_{ABN},[13,25,34] which describes the variation of the parameter ξ as

$$\xi(A_xB_{1-x}N) = x\xi(AN) + (1-x)\xi(BN) - x(1-x)b_{ABN}. \tag{8}$$

The key bowing parameters which have been proposed for wurtzite ternary III-N compounds are listed in Table II.

For quaternary alloys, Glisson *et al.*[35] proposed an expression to interpolate the values of the ternaries, including bowing, in order to obtain a better approximation than the one provided by a simple Végard's approach. This interpolation formula has been commonly used in previous works to deal with the quaternary.[35–37] We use the notation introduced by Chen:[37]

$$\xi(\mathrm{Al}_x\mathrm{In}_y\mathrm{Ga}_z\mathrm{N}) = \frac{xy\xi^u(\mathrm{AlInN}) + yz\xi^v(\mathrm{InGaN}) + xz\xi^w(\mathrm{AlGaN})}{xy + yz + xz}, \tag{9}$$

TABLE II. Bowing parameters for wurtzite III-N ternaries used in this paper, taken from Ref. 25 unless otherwise specified.

	InGaN	AlGaN	AlInN
E_g (eV)	1.4[a]	0.7	5.0[a]
P_{sp} (C/m^2)	− 0.037	− 0.021	− 0.070

[a]Reference 29.

with

$$\xi^u = u\xi(\mathrm{InN}) + (1-u)\xi(\mathrm{AlN}) - u(1-u)b_{\mathrm{AlInN}},$$
$$\xi^v = v\xi(\mathrm{GaN}) + (1-v)\xi(\mathrm{InN}) - v(1-v)b_{\mathrm{InGaN}},$$
$$\xi^w = w\xi(\mathrm{GaN}) + (1-w)\xi(\mathrm{AlN}) - w(1-w)b_{\mathrm{AlGaN}},$$
$$u = \frac{1-x+y}{2}, \quad v = \frac{1-y+z}{2}, \quad w = \frac{1-x+z}{2}$$
and $x + y + z = 1.$

There is no data available in the literature that provides a reliable way to include any nonlinear dependence of the elastic constants C_{ij} or the piezoelectric coefficients e_{ij} into the interpolation formulas. Fiorentini *et al.*[13,38] presented a model for ternary compounds that provides in principle a more accurate description of the piezoelectric polarization in a QW as a second order function of the applied basal strain ε_{11}. They provide quadratic formulas to obtain the piezoelectric response for the binaries, and propose the application of Végard's law to those formulas in order to calculate the piezoelectric polarization in the ternaries. As discussed in further detail in Ref. 13, their results for GaN and InN are only valid for compressive strain ($\varepsilon_{11} < 0$), whereas the results for AlN are applicable also for tensile strain.

Figure 1 compares the piezoelectric polarization derived from the formulas given in Ref. 38 by Fiorentini *et al.* to the one expected from Eq. (2) for a QW using the piezoelectric coefficients calculated by Shimada.[26] The elastic constants reported in Ref. 25 are used. From these results one can conclude that, up to relatively high strain ($|\varepsilon_{11}| \lesssim 6\%$), the two approaches do not differ significantly. Therefore, given the large uncertainties concerning the calculation of accurate polarization-related parameters in III-N materials, and the fact that the expressions derived by Fiorentini *et al.*[38] cannot be used for QD systems, we apply here Végard's law to calculate the piezoelectric constants e_{ij} of the alloys using the values of the binaries reported in Ref. 26 by Shimada.

To calculate the bandgap of the materials, we assume $\varepsilon_{11} = \varepsilon_{22} \neq \varepsilon_{33}$ and choose the smaller of the following transition energies:[39]

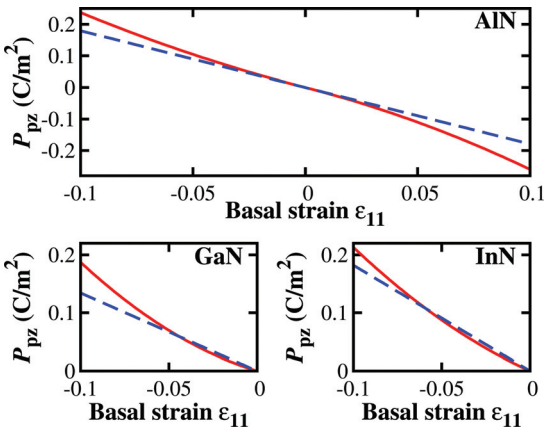

FIG. 1. (Color online) Piezoelectric polarization in nitride binaries. Solid lines indicate the quadratic formulas given in Ref. 38 and dashed lines are Eq. (2) using the piezoelectric coefficients and elastic constants found in Table I.

$$E_{A/B} = E_{A/B}(0) + (a_{cz} - D_1 - D_3)\varepsilon_{33} + 2(a_{ct} - D_2 - D_4)\varepsilon_{11},$$
$$E_C = E_C(0) + (a_{cz} - D_1)\varepsilon_{33} + 2(a_{ct} - D_2)\varepsilon_{11}. \quad (10)$$

Here $E_{A/B}$ denotes the transition energy between the conduction band and the A (heavy hole) and B (light hole) valence bands. Since we have neglected the weak spin-orbit coupling, in the unstrained system, the A- and B-valence bands are degenerate at the Brillouin zone center $[E_A(0) = E_B(0)]$.[40] For the unstrained material, the transition energy between the conduction band and the crystal-field split-off band (C valence band) is given by $E_C(0) = E_{A/B}(0) + \Delta_{cr}$, where Δ_{cr} denotes the crystal-field splitting energy. The valence band deformation potentials are denoted by D_i, while the conduction band deformation potentials are given by a_{cz} and a_{ct}. The values are taken from Yan *et al.*[39] For the crystal-field splitting energy Δ_{cr} we use values of Vurgaftman and Meyer[25] (cf., Table III). Végard's law [Eq. (7)] is applied to obtain the deformation potentials of the ternary and quaternary compounds.

As previously mentioned, in the case of a QD the strain components vary throughout the structure. In line with the surface integral approach[24] employed for the calculation of the piezoelectric potential, we can also use a surface integral approach to obtain the strain in a QD.[41,42] For a truncated-cone shaped dot which is under compressive strain (e.g., GaN/AlN),[43] ε_{11} and ε_{33} follow the trends shown in Fig. 2(a), where a substantial difference can be observed between the strain at the bottom and top interfaces, in contrast to the constant strain across a QW [Fig. 2(b)]. To account for this effect, the values of the strain components ε_{11} and ε_{33} are taken as the value at a half of the dot's height when calculating the bandgap in QD structures. For the barrier, the bandgap value for the "relaxed'' barrier (i.e., far enough from the dot, so that $\varepsilon_{11} = \varepsilon_{33} \approx 0$ is valid) is used.

III. BUILT-IN FIELD REDUCTION

In this section we present a detailed study of the built-in field reduction which can be obtained in ternary and quaternary structures by applying polarization-matched barriers. In a first step, Sec. III A, we introduce the principles behind the concept of polarization matching. In Sec. III B we show the field suppression results for QW and QD systems grown on ideally unstrained barriers, while results for systems with barriers strained to the in-plane lattice constant of an underlying GaN substrate are discussed in Sec. III C. All calculations are performed at room temperature. Quantum size

TABLE III. Deformation potentials for nitride binaries, from Yan *et al.* (Ref. 39). Crystal-field splitting values taken from Vurgaftman and Meyer (Ref. 25).

	GaN	AlN	InN
$a_{cz} - D_1$ (eV)	− 5.81	− 4.31	− 3.62
$a_{ct} - D_2$ (eV)	− 8.92	− 12.11	− 4.60
D_3 (eV)	5.47	9.12	2.68
D_4 (eV)	− 2.98	− 3.79	− 1.74
Δ_{cr} (eV)	0.010	− 0.169	0.040

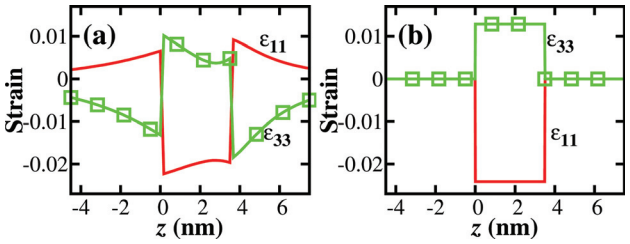

FIG. 2. (Color online) (a) Strain components ε_{11} and ε_{33} (open squares) through the center of a QD along the z direction (parallel to c-axis) for a GaN/AlN truncated-cone shaped dot with height $h = 3.5$ nm, base radius $R_b = 8$ nm (located at $z = 0$) and top radius $R_t = 2$ nm (located at $z = h$) and (b) for a QW of the same height and composition.

effects, which will decrease the effective band offsets and increase the effective transition energies, are not included in this analysis. The exact calculation of these energy shifts is not straightforward as they show a strong dependence on the carrier effective masses as well as the conduction band to valence band offset ratio. The conduction band to valence band offset ratio is still a matter of discussion, with a broad range of different values reported in the literature.[25,29,37,44–47] In addition to this broad spectrum of different values, the interpolation procedure is not well established for quaternary alloys, including the effect of bowing. In view of these uncertainties, we therefore do not attempt to estimate band offsets in this paper. Conventional InGaN/GaN and GaN/AlGaN systems display Type-I band alignment.[48,49] Hums *et al.*[50] report a transition from Type-I to Type-II alignment in GaN/AlInN systems above 25% In content. Since we will be focusing mostly on nearly lattice- and polarization-matched structures, transitivity holds and the band alignment of the presented InGaN/AlInGaN structures is expected to be Type-I up to at least 25% In in the barrier, following Ref. 50. For InGaN/AlInGaN systems above this limit, and AlGaN/AlIn(Ga)N systems (which have not been sufficiently studied to date), Type-II transitions cannot be excluded *a priori*. Taking all these issues into account, further theoretical and experimental investigations on the band offsets in nitride systems are required. This is beyond the scope of this paper. Therefore, we present here the energy gap E_g of the QW (QD) material and the difference in the energy gap ΔE_g between the QW (QD) and the surrounding barrier material as a guide to a particular spectral region, and focus on the relation between built-in field and alloy composition, which is independent of quantum size effects.

A. GaN/AlInN heterostructures

Figure 3 shows the built-in field for a GaN QW (QD) embedded in an AlN (a) or InN (b) matrix, calculated using Eqs. (1) and (4). It can be seen that the resultant built-in field is of opposite sign in the GaN/InN structure compared to the GaN/AlN case, leading to the idea that an *ad hoc* superposition of the curves shown in Figs. 3(a) and 3(b) could lead to effective cancellation of the built-in field.[17] We illustrate this principle here by considering GaN as the well or dot material and $Al_xIn_{1-x}N$ as the barrier material. It can be seen in Figs. 3(a) and 3(b) that the calculated built-in field is in both cases

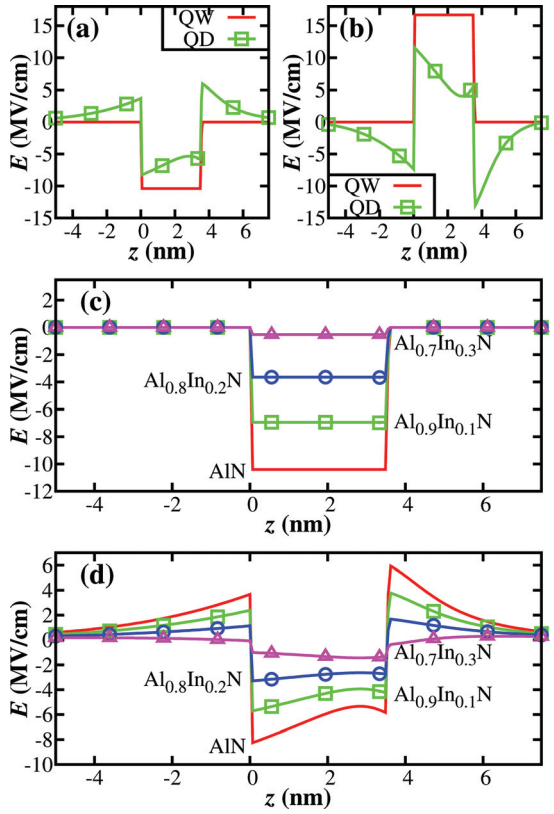

FIG. 3. (Color online) Built-in field along the c axis for (a) GaN/AlN and (b) GaN/InN QD and QW. (c) Built-in field along the c axis for GaN/$Al_xIn_{1-x}N$ QW and (d) QD, as the barrier composition is varied from $x = 1$ to $x = 0.7$. QW and QD of typical dimensions (well: height $h = 3.5$ nm; truncated-cone dot: base radius $R_b = 8$ nm, top radius $R_t = 2$ nm and height $h = 3.5$ nm).

reduced in the QD structure compared to the QW case. This occurs both because of the reduced surface area of a dot compared to a QW (reduced area of induced surface charge) and also because of the reduction in the magnitude of ε_{11} and ε_{33} in the QD structure,[51,52] as seen in Fig. 2. The growth of QDs can therefore provide an additional route to field reduction in c plane III-N heterostructures,[52,53] as recently demonstrated experimentally.[54]

Figures 3(c) and 3(d) depict the calculated built-in field in GaN/$Al_xIn_{1-x}N$ QW and QD structures, showing that a complete suppression of the built-in field can be achieved for $x \approx 0.7$ in both QW and QD structures, at the expense of reducing the initial energy gap difference between dot and barrier from ~2.5 to ~0.3 eV (Fig. 4). This loss of confinement is not critical compared to the potential benefits of reducing the field-induced spatial separation of the carriers.[17]

B. Quaternary structures: Unstrained barriers

We turn now to show how the use of unstrained quaternary barrier structures can enable field reduction for a very wide range of QW and QD bandgap energies, supporting efficient optical emission across a wide wavelength range. We use the interpolation formulas from Sec. II B, and illustrate the method by considering the range of polarization-matched barriers which can be achieved with an $In_{0.3}Ga_{0.7}N$/$Al_xIn_yGa_{1-x-y}N$ QW system. The colored contours in the top panel in Fig. 5 show the calculated built-in field across an $In_{0.3}Ga_{0.7}N$ QW as a function of unstrained barrier quaternary composition, while the contours in the bottom panel show the calculated energy gap of the $In_{0.3}Ga_{0.7}N$ QW strained to the barrier lattice constant. The solid lines in both panels show the difference in energy gap, ΔE_g, between the QW and surrounding barrier layer.

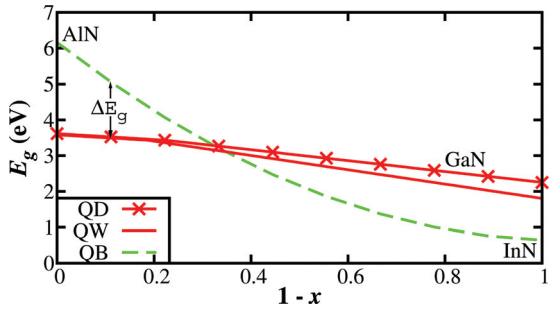

FIG. 4. (Color online) Variation of the bandgap difference ΔE_g (at room temperature) between the GaN QD or QW and the $Al_xIn_{1-x}N$ barrier (QB) as x decreases in the GaN/$Al_xIn_{1-x}N$ system. The same dot dimensions are assumed as in Fig. 3.

A whole range of barrier compositions (characterized by the white area in the top panel) is found to effectively suppress the field, and the energy gap of $In_{0.3}Ga_{0.7}N$ is observed to be fixed around 2.25 eV for that range (bottom panel).

In the most general case, a quaternary alloy can be employed in both well (dot) and barrier. Doing so, the system gains additional degrees of freedom that allow, for a given bandgap E_g, to minimize the built-in field value and maximize the bandgap difference ΔE_g between well and barrier. Figure 6 (top) shows a schematic illustration of the optimization procedure used to calculate the system composition, compatible with certain E_g and ΔE_g, for which the built-in field is minimum. As an example, the calculated minimum built-in field as a function of energy gap difference, ΔE_g, between a strained QW or QD with 2.25 eV energy gap and an unstrained barrier layer is shown in Fig. 6 (bottom). In this case, it is possible to achieve a maximum offset close to 0.3 eV in both the QD and QW cases. We note for larger offsets that the absolute value of the minimum built-in field achievable is generally smaller in the QD than the QW case, as expected from the earlier discussion of Figs. 3(a) and 3(b). Table IV shows the calculated QW/barrier and QD/barrier compositions of built-in field-free systems which maximize the offset ΔE_g between the strained QW (QD) structure and unstrained barrier layers, as a function of increasing strained QW or QD energy gap. In the case of $E_g = 2.25$ eV this corresponds to the last zero-field point in Fig. 6 (bottom). The table also shows the lattice mismatch between the QW (QD) and barrier materials. In the case of the QW, the lattice mismatch equals ε_{11} and in the case of the QD it equals the in-plane initial misfit strain $\varepsilon_{0,a}$.[24]

C. Pseudomorphic barriers on a GaN substrate

In addition to the structures with unstrained barriers, we consider here also systems where both the barrier and the QW (QD) materials are grown pseudomorphically on a substrate with a different lattice constant. Therefore, this analysis gives

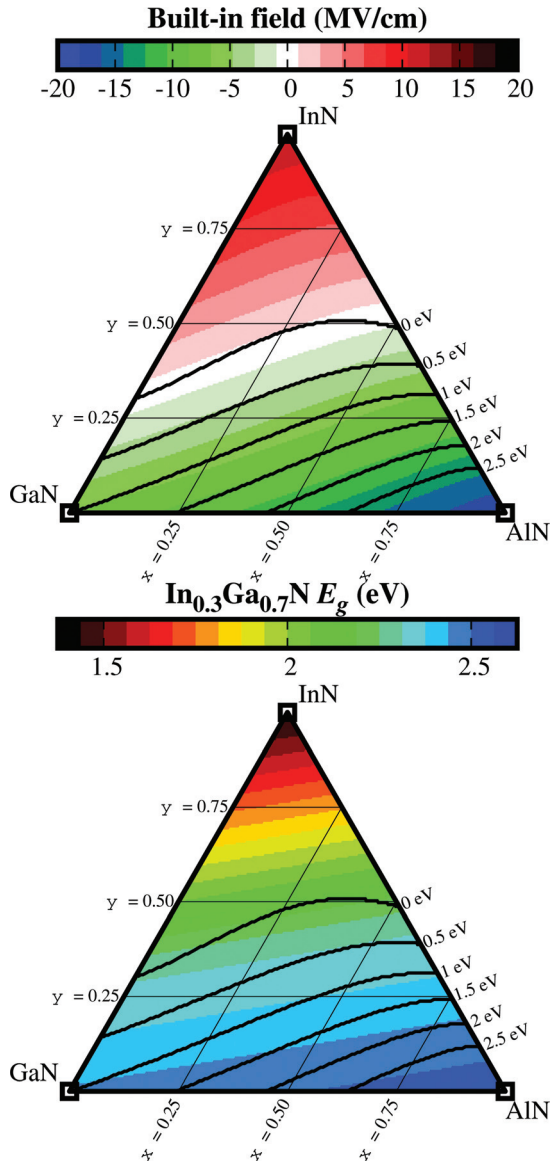

FIG. 5. (Color online) (Top) Calculated built-in field for an $In_{0.3}Ga_{0.7}N/Al_xIn_yGa_{1-x-y}N$ QW system and (bottom) energy gap E_g, at room temperature, of the $In_{0.3}Ga_{0.7}N$ layer as the barrier composition (and hence strain) varies. The thick solid lines indicate the bandgap difference ΔE_g between well and barrier.

an insight into the behavior of the built-in fields when the barrier exhibits residual strain due to an underlying substrate. Since nitride-based heterostructures are commonly grown on a GaN buffer layer, we investigate here the compositions and strains required for field-matched QW/barrier and QD/barrier structures grown on an unstrained GaN epilayer. A similar approach was also used in Refs. 17 and 37. In general, both the barrier and QW (QD) layers will be strained in such structures, so that the piezoelectric charges and hence the built-in field will be modified compared to the previous case.

Since the barrier material is strained to the GaN buffer layer, the total built-in polarization of the barrier material is no longer given by the spontaneous polarization only. Here, the (spontaneous) polarization of the barrier material in Eqs. (1) and (4) has to be replaced by

$$P^{\mathrm{B}}_{\mathrm{tot}} = P^{\mathrm{B}}_{\mathrm{sp}} + P^{\mathrm{B}}_{\mathrm{pz}}. \tag{11}$$

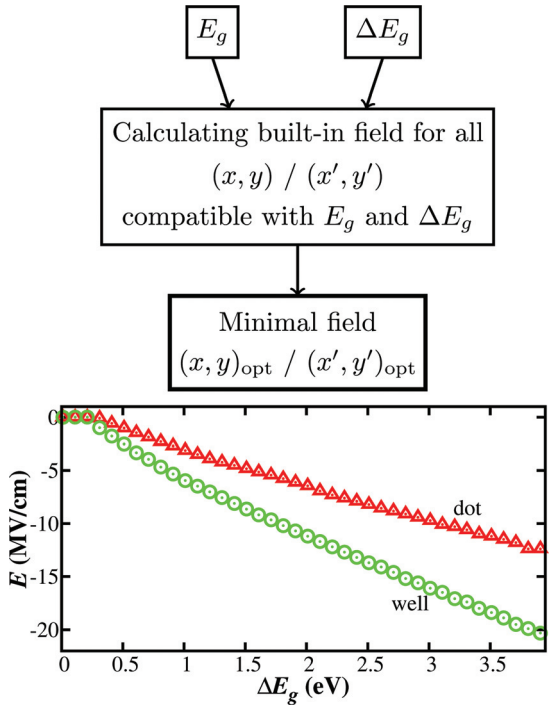

FIG. 6. (Color online) (top) Flux diagram explaining how, for a certain combination of E_g and ΔE_g at room temperature, the compositions of the $Al_xIn_yGa_{1-x-y}N/Al_{x'}In_{y'}Ga_{1-x'-y'}N$ system that minimize the built-in field are obtained and (bottom) smallest built-in field that can be obtained for a QW and a QD system where $E_g = 2.25$ eV as the bandgap difference ΔE_g between the barrier and well (or dot) increases.

P^{B}_{pz} can be obtained from Eq. (2), assuming that the basal strain applied to the barrier is given by

$$\varepsilon^{\mathrm{B}}_{11} = \frac{a^{\mathrm{GaN}} - a^{\mathrm{B}}_0}{a^{\mathrm{B}}_0}, \tag{12}$$

where a^{B}_0 and a^{GaN} refer to the a lattice constant of the fully relaxed barrier material and of GaN, respectively. To obtain the piezoelectric polarization in the well, only the consideration that it is strained in the basal plane to the GaN lattice constant a^{GaN} instead of a^{B}_0 has to be made:

$$\varepsilon^{\mathrm{W}}_{11} = \frac{a^{\mathrm{GaN}} - a^{\mathrm{W}}_0}{a^{\mathrm{W}}_0}. \tag{13}$$

In both cases, the ε_{33} component of the strain is then given by Eq. (3).

As pointed out previously, when basal strain alone is applied to a material layer, a relaxation takes place in the [0001] direction (perpendicular to that plane) as given by Eq. (3). When dealing with the QD in the strained barrier case, this relaxation will imply a change in the effective lattice constants of the barrier. Therefore, to calculate the strain and the built-in field in such a system, we proceed in the following way. First, the dot embedded in an unstrained barrier will be considered and the surface integral method is used to obtain the built-in field profile as described in Sec. III B. Second, the basal strain corresponding to the introduction of the GaN buffer layer will be added and the previous structure will be assumed to follow the relaxation mechanisms of the barrier alone, as expected

TABLE IV. List of QW and QD $Al_xIn_yGa_{1-x-y}N/Al_{x'}In_{y'}Ga_{1-x'-y'}N$ systems compatible with zero built-in field that, for a given E_g at room temperature, maximize the band gap difference ΔE_g between well (dot) and barrier. The lattice mismatch is $(a_B - a_{D/W})/a_{D/W}$ for the unstrained barrier case, and $(a_{GaN} - a_{D/W})/a_{D/W}$ for the dot or well and $(a_{GaN} - a_B)/a_B$ for the barrier in the case of pseudomorphic growth on a GaN buffer layer.

	QW				QD			
E_g (eV)	ΔE_g (eV)	$(x,y)_{opt}/(x',y')_{opt}$	Lattice mismatch (%)		ΔE_g (eV)	$(x,y)_{opt}/(x',y')_{opt}$	Lattice mismatch (%)	
			Unstrained barriers					
2.00	0.24	(0.46,0.54)/(0.25,0.46)	−0.4		0.32	(0.43,0.57)/(0.03,0.32)		−1.7
2.25	0.22	(0.51,0.49)/(0.32,0.42)	−0.3		0.31	(0.50,0.50)/(0.27,0.37)		−0.9
2.50	0.20	(0.55,0.45)/(0.36,0.38)	−0.3		0.29	(0.54,0.46)/(0.32,0.34)		−0.8
2.75	0.21	(0.00,0.13)/(0.43,0.34)	1.3		0.27	(0.58,0.42)/(0.36,0.30)		−0.8
3.00	0.27	(0.01,0.06)/(0.51,0.30)	1.5		0.25	(0.62,0.38)/(0.42,0.27)		−0.7
3.25	0.32	(0.02,0.00)/(0.52,0.24)	1.5		0.24	(0.66,0.34)/(0.48,0.24)		−0.7
3.50	0.31	(0.13,0.00)/(0.58,0.22)	1.4		0.22	(0.69,0.31)/(0.51,0.21)		−0.7
3.75	0.30	(0.23,0.00)/(0.64,0.20)	1.2		0.20	(0.72,0.28)/(0.53,0.17)		−0.8
4.00	0.28	(0.33,0.00)/(0.70,0.18)	1.1		0.18	(0.76,0.24)/(0.62,0.16)		−0.6
			Pseudomorphic growth on GaN					
			Well	Barrier			Dot	Barrier
2.00	0.31	(0.42,0.58)/(0.32,0.52)	−5.2	−4.8	0.18	(0.42,0.58)/(0.24,0.53)	−5.2	−5.1
2.25	0.29	(0.00,0.36)/(0.37,0.47)	−3.9	−4.2	0.19	(0.47,0.53)/(0.31,0.48)	−4.6	−4.4
2.50	0.30	(0.00,0.28)/(0.41,0.42)	−3.0	−3.6	0.19	(0.51,0.49)/(0.28,0.40)	−4.1	−3.7
2.75	0.32	(0.00,0.20)/(0.46,0.37)	−2.2	−2.9	0.19	(0.56,0.44)/(0.38,0.37)	−3.4	−3.1
3.00	0.34	(0.01,0.13)/(0.49,0.32)	−1.4	−2.3	0.19	(0.60,0.40)/(0.43,0.33)	−2.9	−2.6
3.25	0.37	(0.00,0.05)/(0.58,0.29)	−0.6	−1.8	0.19	(0.63,0.37)/(0.36,0.23)	−2.5	−1.7
3.50	0.39	(0.04,0.00)/(0.62,0.25)	0.1	−1.3	0.20	(0.67,0.33)/(0.49,0.24)	−2.0	−1.5
3.75	0.36	(0.17,0.00)/(0.65,0.22)	0.4	−0.9	0.20	(0.71,0.29)/(0.51,0.18)	−1.5	−0.8
4.00	0.31	(0.30,0.00)/(0.68,0.18)	0.7	−0.4	0.18	(0.75,0.25)/(0.56,0.14)	−1.0	−0.2

from Eqs. (12) and (3). Therefore, the additional contribution to the QD built-in potential φ^{QD} in Eq. (4) will be

$$\Delta\varphi^{QD} = \frac{\Delta P^D_{pz} - \Delta P^B_{pz}}{4\pi\varepsilon_0\varepsilon_r} I_2, \tag{14}$$

with the additional introduced piezoelectric polarization being

$$\Delta P^D_{pz} = 2e^D_{31}\Delta\varepsilon^D_{11} + e^D_{33}\Delta\varepsilon^D_{33} \tag{15}$$

and

$$\Delta P^B_{pz} = 2e^B_{31}\Delta\varepsilon^B_{11} + e^B_{33}\Delta\varepsilon^B_{33}, \tag{16}$$

where we have assumed

$$\Delta\varepsilon^D_{11} = \Delta\varepsilon^B_{11}, \qquad \Delta\varepsilon^D_{33} = \Delta\varepsilon^B_{33}, \tag{17}$$

and

$$\Delta\varepsilon^B_{11} = \frac{a^{GaN} - a^B_0}{a^B_0}, \qquad \Delta\varepsilon^B_{33} = -2\frac{C^B_{13}}{C^B_{33}}\Delta\varepsilon^B_{11}. \tag{18}$$

Compared to the previous case with unstrained barriers, pseudomorphic growth on a GaN epilayer allows similar results, as can be seen in Fig. 7, which shows the calculated minimum field achievable as a function of bandgap difference, ΔE_g, between the QW (QD) and barrier layer for $E_g = 2.25$ eV in the QW (QD) region. Table IV shows the calculated QW/barrier and QD/barrier compositions as a function of increasing QW (QD) energy gap to maximize the offset ΔE_g between the strained QW (QD) and strained barrier layers. The table also shows the lattice mismatch in the QW (QD) and the barrier layers. The additional contribution to the strain assumed in Eq. (17) is found to be of a higher order of magnitude than the main contribution to the strain field modeled via Eq. (5) for the low energy gap structures in the right hand side of Table IV. For the sake of completeness, and to be able to compare these results with those obtained in the previous section, we have included the results for the lower-gap structures ($E_g \lesssim 3.5$ eV), even though these systems are impractical to grow, given the large lattice mismatch between the GaN substrate and the barrier layers. For $E_g = 3.5$ eV and above, the mismatch is within the range which could probably be accommodated to allow pseudomorphic growth on GaN. In this range, the contributions to the field from Eqs. (5) and (17) are found to be of the same order and therefore our approximation should be more accurate within that range. As discussed in the Introduction, a built-in field reduction in systems with $E_g \geq 3.5$ eV, is of strong interest for applications operating in the UV spectral range.[55,56]

D. Strain and miscibility limitations to built-in field suppression

The structures studied in Secs. III B and III C, and listed in Table IV, depict a best-case scenario for the growth of III-N heterostructures where the intrinsic built-in field has been calculated to vanish, while maximizing the energy gap difference between the barrier and well or dot layers. However, these results do not consider any constraints encountered during the epitaxial growth of nitride-based heterostructures. Particularly, the amount of In that can be incorporated into InGaN and AlInN alloys while maintaining high crystal quality is currently for layered structures about 30% in both

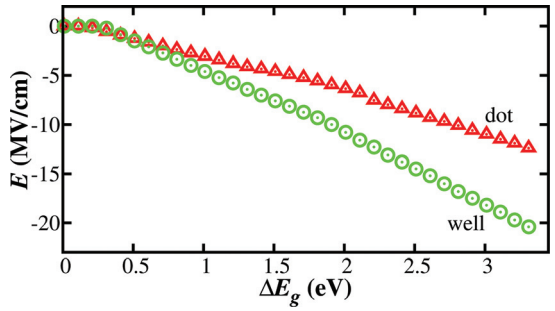

FIG. 7. (Color online) Lowest built-in field achievable, as a function of ΔE_g, for a QD and a QW system grown on a GaN substrate for which $E_g = 2.25$ eV.

cases.[4,57–61] In the case of QDs, higher In contents of up to $\sim 35\%$ have been reported in InGaN QDs,[62,63] whereas AlInN QDs have not been studied significantly in the literature. Regarding strain, devices with as much as $\sim 1.1\%$ compressive in-plane strain in the barriers along the whole active layer have been reported.[23] For InGaN/GaN QWs and QDs, strain (lattice mismatch in the case of QD) of up to 3% and 3.8%, respectively, can be found in the literature.[4,23,57,62,63] Hence, the calculated strains in the top half of Table IV for QW growth between unstrained barriers are all within the limits achieved experimentally. Turning to the structures grown on GaN in the bottom half of Table IV, built-in field reduction in these cases requires similar values for the strain in both the QW and the barrier. Therefore, the strain state of the barrier material is the one that sets a limit to the possible structures. In both halves of Table IV, the built-in field minimization procedure yields AlInN QDs as the optimal structures. This initially surprising result is due to the large bandgap bowing of AlInN compared to InGaN. For high In contents, the bandgap of AlInN is very similar to the bandgap of InGaN, as shown in Ref. 29. Therefore, in terms of built-in field reduction, AlInN QD systems could be more suitable than InGaN QDs. However, as previously mentioned, these AlInN systems have not been explored in detail and significant challenges remain for their experimental realization.

To realistically model the possible built-in field reduction in QW and QD systems, the optimization procedure of Sec. III B and III C can be repeated to take all the constraints discussed above into account. The resultant structures, optimized in terms of built-in field reduction and maximization of bandgap difference ΔE_g are shown in Table V. The calculations have been made imposing a minimum value of $\Delta E_g = 0.25$ eV for QWs and $\Delta E_g = 0.30$ eV for QDs, because of the higher confinement energy expected in QDs compared to QWs, that would reduce the effective bandgap offset.

As can be seen from the data in Table V, the imposition of such constraints sets a limit to the built-in field suppression, especially for those structures with low energy gaps (typically around and below 3 eV). However, it is always possible to achieve at least a partial field reduction in those structures, which has already been shown to have a significant impact on the efficiency of LED devices.[23] For the rest of the structures, a complete built-in field suppression is possible and, in line with the results reported in Ref. 23, an improved performance is expected by incorporating them into devices that span a wavelength range which extends well into the UV part of the spectrum.

TABLE V. List of $Al_xIn_yGa_{1-x-y}N/Al_{x'}In_{y'}Ga_{1-x'-y'}N$ systems compatible with the constraints discussed in Sec. III D: 30% maximum In content for QWs and QBs; 35% maximum In content in QDs; 3% maximum strain in QWs; 3.8% maximum strain (lattice mismatch) in QDs; 1.1% maximum strain in QBs; 0.25 eV minimum ΔE_g for QWs; and 0.3 eV minimum ΔE_g for QDs. Note that in the case of a QW system an energy gap of 2.25 and 2.5 eV, for unstrained barriers and pseudomorphic growth on GaN respectively, is not compatible with the given constraints.

	QW					QD				
E_g (eV)	E_{b-i}(MV/cm)	ΔE_g (eV)	$(x,y)_{opt}/(x',y')_{opt}$	Lattice mismatch (%)		E_{b-i}(MV/cm)	ΔE_g (eV)	$(x,y)_{opt}/(x',y')_{opt}$	Lattice mismatch (%)	
				Unstrained barriers						
2.25	n/a	n/a	n/a	n/a		− 1.1	0.31	(0.00,0.35)/(0.01,0.23)		− 1.3
2.50	− 1.4	0.26	(0.00,0.24)/(0.19,0.27)	− 0.1		− 1.0	0.30	(0.02,0.29)/(0.00,0.16)		− 1.4
2.75	− 0.7	0.25	(0.00,0.15)/(0.33,0.28)	0.6		− 1.0	0.30	(0.01,0.21)/(0.03,0.11)		− 1.1
3.00	0.0	0.27	(0.00,0.06)/(0.48,0.29)	1.4		− 1.0	0.30	(0.03,0.13)/(0.23,0.15)		− 0.3
3.25	0.0	0.32	(0.00,0.00)/(0.49,0.23)	1.4		− 0.8	0.30	(0.03,0.02)/(0.47,0.22)		1.2
3.50	0.0	0.31	(0.11,0.00)/(0.53,0.20)	1.2		− 0.8	0.30	(0.10,0.00)/(0.51,0.19)		1.1
3.75	0.0	0.30	(0.23,0.00)/(0.64,0.20)	1.2		− 0.8	0.30	(0.19,0.00)/(0.52,0.14)		0.8
4.00	0.0	0.28	(0.33,0.00)/(0.70,0.18)	1.1		− 0.8	0.30	(0.29,0.00)/(0.57,0.11)		0.6
				Pseudomorphic growth on GaN						
				Well	barrier				Dot	barrier
2.50	n/a	n/a	n/a	n/a	n/a	− 2.1	0.59	(0.02,0.33)/(0.01,0.10)	− 3.5	− 1.1
2.75	− 2.2	0.35	(0.00,0.20)/(0.01,0.10)	− 2.2	− 1.1	− 1.2	0.34	(0.00,0.22)/(0.01,0.10)	− 2.4	− 1.1
3.00	− 1.2	0.25	(0.01,0.13)/(0.12,0.12)	− 1.4	− 1.0	− 0.9	0.30	(0.03,0.15)/(0.16,0.13)	− 1.6	− 1.1
3.25	− 0.4	0.27	(0.00,0.05)/(0.30,0.16)	− 0.6	− 1.1	− 0.6	0.30	(0.01,0.05)/(0.33,0.17)	− 0.5	− 1.1
3.50	0.0	0.36	(0.04,0.00)/(0.52,0.21)	0.1	− 1.1	− 0.5	0.30	(0.05,0.00)/(0.47,0.20)	0.1	− 1.1
3.75	0.0	0.36	(0.17,0.00)/(0.63,0.21)	0.4	− 0.8	− 0.6	0.31	(0.16,0.00)/(0.56,0.19)	0.4	− 0.8
4.00	0.0	0.31	(0.30,0.00)/(0.68,0.18)	0.7	− 0.4	− 0.8	0.30	(0.29,0.00)/(0.64,0.16)	0.7	− 0.2

IV. SUMMARY

In summary, we have shown that it is in principle possible for a very wide range of emission energies to reduce or even completely suppress the high built-in fields intrinsic to wurtzite III-N heterostructures. This is achieved by taking advantage that the built-in field is of opposite sign across the GaN layer in InN/GaN/InN and in AlN/GaN/AlN structures. The built-in field can then be minimized and a significant energy gap difference ΔE_g can be maintained by a careful choice of the alloy composition in the QW (QD) and barrier layers. We have presented the calculated QW (QD) and barrier systems to maintain zero field and maximize ΔE_g across a large range of QW (QD) energy gap values. Results were presented both for unstrained barriers and also for QW/barrier and QD/barrier structures grown pseudomorphically on a GaN substrate. Furthermore, we have discussed and considered in our calculations several constraints (miscibility issues, strain limitations) set by the epitaxial growth of III-N semiconductors. The built-in strain in each of the structures considered is also presented. Interpolation between the QW (QD) and barrier compositions can then be used to estimate the maximum offset for a given energy gap as a function of built-in strain in the QW (QD) and barrier layers. Overall, we have noted uncertainties in several critical material parameters, including in particular the strain and composition dependence of piezoelectric coefficients. Further theoretical and experimental effort is required to reduce the uncertainty in these values. We conclude that growth of suitable ternary and quaternary alloy combinations, in particular AlInN with high In content, has the potential to significantly reduce the built-in electric field in *c*-plane III-N heterostructures, of considerable benefit for a wide range of optoelectronic applications.

ACKNOWLEDGMENTS

The authors would like to thank Peter Parbrook for fruitful discussions. This work was supported by Science Foundation Ireland and by the IRCSET Empower post-doctoral fellowship scheme (SS).

[1]C. J. Humphreys, MRS Bull. **33**, 459 (2008).
[2]M. Yamada, T. Mitani, Y. Narukawa, S. Shioji, I. Niki, S. Sonobe, K. Deguchi, M. Sano, and T. Mukai, Jpn. J. Appl. Phys. **41**, L1431 (2002).
[3]M. R. Krames, O. B. Shchekin, R. Mueller-Mach, G. O. Mueller, L. Zhou, G. Harbers, and M. G. Craford, J. Disp. Technol. **3**, 160 (2007).
[4]P. T. Barletta, E. A. Berkman, B. F. Moody, N. A. El-Masry, A. M. Emara, M. J. Reed, and S. M. Bedair, Appl. Phys. Lett. **90**, 151109 (2007).
[5]M. Zhu, S. You, T. Detchprohm, T. Paskova, E. A. Preble, and C. Wetzel, Phys. Status Solidi A **207**, 1305 (2010).
[6]M. A. Khan, M. Shatalov, H. P. Maruska, H. M. Wang, and E. Kuokstis, Jpn. J. Appl. Phys. **44**, 7191 (2005).
[7]Y. Taniyasu, M. Kasu, and T. Makimoto, Nature **441**, 325 (2006).
[8]J. R. Grandusky, J. A. Smart, M. C. Mendrick, L. J. Schowalter, K. X. Chen, and E. F. Schubert, J. Cryst. Growth **311**, 2864 (2009).
[9]T. Matsuoka, Superlattices Microstruct. **37**, 19 (2005).
[10]S. V. Novikov, C. T. Foxon, T. S. Cheng, T. L. Tansley, J. W. Orton, D. E. Lacklison, D. Johnston, N. Baba-Ali, S. E. Hooper, L. C. Jenkins, L. Eaves J. Cryst. Growth **146**, 340 (1995).
[11]S. V. Novikov, N. M. Stanton, R. P. Campion, R. D. Morris, H. L. Geen, C. T. Foxon, and A. J. Kent, Semicond. Sci. Technol. **23**, 015018 (2008).
[12]K. Kim, W. R. L. Lambrecht, and B. Segall, Phys. Rev. B **53**, 16310 (1996).
[13]O. Ambacher, J. Majewski, C. Miskys, A. Link, M. Hermann, M. Eickhoff, M. Stutzmann, F. Bernardini, V. Fiorentini, V. Tilak, B. Schaff, and L. F. Eastman, J. Phys.: Condens. Matter **14**, 3399 (2002).
[14]T. Paskova, Phys. Status Solidi B **245**, 1011 (2008).
[15]Y. C. Shen, G. O. Mueller, S. Watanabe, N. F. Gardner, A. Munkholm, and M. R. Krames, Appl. Phys. Lett. **91**, 141101 (2007).
[16]B. Monemar and B. E. Sernelius, Appl. Phys. Lett. **91**, 181103 (2007).
[17]M.-H. Kim, M. F. Schubert, Q. Dai, J. K. Kim, E. F. Schubert, J. Piprek, and Y. Park, Appl. Phys. Lett. **91**, 183507 (2007).
[18]M. F. Schubert and E. F. Schubert, Appl. Phys. Lett. **96**, 131102 (2010).
[19]A. D. Andreev and E. P. O'Reilly, Appl. Phys. Lett. **79**, 521 (2001).
[20]N. Baer, S. Schulz, S. Schumacher, P. Gartner, G. Czycholl, and F. Jahnke, Appl. Phys. Lett. **87**, 231114 (2005).
[21]H. J. Chung, R. J. Choi, M. H. Kim, J. W. Han, Y. M. Park, Y. S. Kim, H. S. Paek, C. S. Sone, Y. J. Park, J. K. Kim, E. F. Schubert, Appl. Phys. Lett. **95**, 241109 (2009).
[22]J. Xu, M. F. Schubert, A. N. Noemaun, D. Zhu, J. K. Kim, E. F. Schubert, M. H. Kim, H. J. Chung, S. Yoon, C. Sone, Y. Park, Appl. Phys. Lett. **94**, 011113 (2009).
[23]W. Lee, M.-H. Kim, D. Zhu, A. N. Noemaun, J. K. Kim, and E. F. Schubert, J. Appl. Phys. **107**, 063102 (2010).
[24]D. P. Williams, A. D. Andreev, E. P. O'Reilly, and D. A. Faux, Phys. Rev. B **72**, 235318 (2005).
[25]I. Vurgaftman and J. R. Meyer, J. Appl. Phys. **94**, 3675 (2003).
[26]K. Shimada, Jpn. J. Appl. Phys. **45**, L358 (2006).
[27]J.-M. Wagner and F. Bechstedt, Phys. Rev. B **66**, 115202 (2002).
[28]J. Furthmüller, P. H. Hahn, F. Fuchs, and F. Bechstedt, Phys. Rev. B **72**, 205106 (2005).
[29]J. Wu, J. Appl. Phys. **106**, 011101 (2009).
[30]S. Schulz, A. Berube, and E. P. O'Reilly, Phys. Rev. B **79**, 081401(R) (2009).
[31]H. Shen, M. Wraback, H. Zhong, A. Tyagi, S. P. DenBaars, S. Nakamura, and J. S. Speck, Appl. Phys. Lett. **95**, 033503 (2009).
[32]F. Bernardini and V. Fiorentini, Phys. Status Solidi A **190**, 65 (2002).
[33]M. Winkelnkemper, A. Schliwa, and D. Bimberg, Phys. Rev. B **74**, 155322 (2006).
[34]F. Bernardini and V. Fiorentini, Phys. Rev. B **64**, 085207 (2001).
[35]T. H. Glisson, J. R. Hauser, M. A. Littlejohn, and C. K. Williams, J. Electron. Mater. **7**, 1 (1978).
[36]I. Vurgaftman, J. R. Meyer, and L. R. Ram-Mohan, J. Appl. Phys. **89**, 5815 (2001).
[37]J.-R. Chen, S.-C. Ling, H.-M. Huang, P.-Y. Su, T.-S. Ko, T.-C. Lu, H.-C. Kuo, Y.-K. Kuo, and S.-C. Wang, Appl. Phys. B **95**, 145 (2009).
[38]V. Fiorentini, F. Bernardini, and O. Ambacher, Appl. Phys. Lett. **80**, 1204 (2002).
[39]Q. Yan, P. Rinke, M. Scheffler, and C. G. Van de Walle, Appl. Phys. Lett. **95**, 121111 (2009).
[40]S. Schulz, S. Schumacher, and G. Czycholl, Eur. Phys. J. B **64**, 51 (2008).
[41]J. R. Downes, D. A. Faux, and E. P. O'Reilly, J. Appl. Phys. **81**, 6700 (1997).
[42]J. H. Davies, J. Appl. Phys. **84**, 1358 (1998).
[43]The convention in this paper is to refer to the dot or well before the barrier, i.e., ''GaN/AlN′'' refers to either a GaN dot or well embedded in an AlN barrier.
[44]H. Zhang, E. J. Miller, E. T. Yu, C. Poblenz, and J. S. Speck, Appl. Phys. Lett. **84**, 4644 (2004).
[45]S. Nicolay, J.-F. Carlin, E. Feltin, R. Butté, M. Mosca, N. Grandjean, M. Ilegems, M. Tchernycheva, L. Nevou, and F. H. Julien, Appl. Phys. Lett. **87**, 111106 (2005).
[46]P. D. C. King, T. D. Veal, C. E. Kendrick, L. R. Bailey, S. M. Durbin, and C. F. McConville, Phys. Rev. B **78**, 033308 (2008).
[47]S. Schulz, T. J. Badcock, M. A. Moram, P. Dawson, M. J. Kappers, C. J. Humphreys, and E. P. O'Reilly, Phys. Rev. B **82**, 125318 (2010).
[48]P. G. Moses and C. G. Van de Walle, Appl. Phys. Lett. **96**, 021908 (2010).
[49]S. L. Chuang and C. S. Chang, Semicond. Sci. Technol. **12**, 252 (1997).
[50]C. Hums, A. Gadanecz, A. Dadgar, J. Bläsing, P. Lorenz, S. Krischok, F. Bertram, A. Franke, J. A. Schaefer, J. Christen, and A. Krost, Phys. Status Solidi C **6**, S451 (2009).
[51]D. P. Williams, S. Schulz, A. D. Andreev, and E. P. O'Reilly, IEEE J. Sel. Top. Quantum Electron. **15**, 1092 (2009).
[52]S. Schulz and E. P. O'Reilly, Phys. Rev. B **82**, 033411 (2010).
[53]Y.-R. Wu, Y.-Y. Lin, H.-H. Huang, and J. Singh, J. Appl. Phys. **105**, 013117 (2009).
[54]M. Zhang, P. Bhattacharya, and W. Guo, Appl. Phys. Lett. **97**, 011103 (2010).

[55]Y.-K. Kuo, S.-H. Yen, and Y.-W. Wang, Proc. SPIE **6669**, 66691J (2007).
[56]M. S. Shur and R. Gaska, Proc. SPIE **6894**, 689419 (2008).
[57]H. Zhao, G. Liu, X.-H. Li, G. S. Huang, J. D. Poplawsky, S. T. Penn, V. Dierolf, and N. Tansu, Appl. Phys. Lett. **95**, 061104 (2009).
[58]T.-T. Kang, M. Yamamoto, M. Tanaka, A. Hashimoto, and A. Yamamoto, J. Appl. Phys. **106**, 053525 (2009).
[59]L. Kirste, T. Lim, R. Aidam, S. Müller, P. Waltereit, and O. Ambacher, Phys. Status Solidi A **207**, 1338 (2010).
[60]K. Lorenz, S. Magalhães, N. Franco, N. P. Barradas, V. Darakchieva, E. Alves, S. Pereira, M. R. Correia, F. Munnik, R. W. Martin, K. P. O'Donnell, I. M. Watson, Phys. Status Solidi B **247**, 1740 (2010).
[61]C. Hums, J. Bläsing, A. Dadgar, A. Diez, T. Hempel, J. Christen, A. Krost, K. Lorenz, and E. Alves, Appl. Phys. Lett. **90**, 022105 (2007).
[62]C. Adelmann, J. Simon, G. Feuillet, N. T. Pelekanos, B. Daudin, and G. Fishman, Appl. Phys. Lett. **76**, 1570 (2000).
[63]O. Moriwaki, T. Someya, K. Tachibana, S. Ishida, and Y. Arakawa, Appl. Phys. Lett. **76**, 2361 (2000).